# Unraveling the Organotellurium Chemistry Applied to the Synthesis of Gold Nanomaterials.

**Javier Fernández-Lodeiro*[a,b,d], Benito Rodríguez-González,[c] Hugo M. Santos,[a,b] Emilia Bertolo,[e] José Luis Capelo,[a,b] Alcindo A. Dos Santos*[d] and Carlos Lodeiro*[a,b]**

[a]*BIOSCOPE Group, UCIBIO@REQUIMTE, Chemistry Department, Faculty of Science and Technology, University NOVA of Lisbon, Caparica, 2829-516, Portugal.*

[b]*ProteoMass Scientific Society, Madan Parque, Building VI, Office 23, Faculty of Science and Technology, Campus de Caparica, 2829-516. Caparica. Portugal.*

[c]*Scientific and Technological Research Assistance Centre (CACTI), University of Vigo, Lagoas-Marcosende, Vigo, Spain*

[d]*Instituto de Química, Universidade de São Paulo, Av. Prof. Lineu Prestes, 748, CxP.26077, São Paulo 05508-000, Brazil.*

[e]*Biomolecular Research Group, School of Human and Life Sciences, Canterbury Christ Church University, Canterbury CT1 1QU, United Kingdom*

**1. Materials.** Hydrogen tetrachloroaurate(III) trihydrate (99.99 % metal basis) (CAS:16961-25-4) was purchased from Alfa Aesar. Diphenyl ditelluride (98%) (CAS: 32294-60-3), Calcium hydride (95%) (CAS: 7789-78-8), 4-mercaptophenylacetic acid (99%) (CAS: 39161-84-7), Tetraethyl orthosilicate (99.99%) (CAS: 78-10-4), Ammonium hydroxide (CAS: 1336-21-6) were purchased from Sigma-Aldrich. Poly(acrylic acid) sodium salt (MW 6000) was purchased from Polyscience. Solvents, HPLC Plus grade, were purchased from Carlo Erba. Acetonitrile for the syntheses was pre-dried by shaking with 4A molecular sieves, and then distilled over calcium hydride. Bovine serum albumin (BSA) Carbonic Anydrase (CA), N,N,N,N′-tetramethylethylene-diamine (TMED), glycine, β-mercaptoethanol, glycerol 86–88%, coomassie blue R-250 (CBB), DL-dithiotreitol (DTT), iodoacetamide (IAA), acrylamide/bis- acrylamide 30% solution (37.5:1) and ammonium persulfate were purchased from Sigma-Aldrich (Basel, Switzerland). Hydrochloric acid (HCl), tris–base, sodium dodecyl sulphate (SDS), and methanol were purchased from Panreac (Barcelona, Spain). Bromophenol blue was from Riedel-de Haën (Basel, Switzerland). Molecular weight marker for gel

electrophoresis Precision Plus Protein™ All Blue was purchased from Bio-Rad (USA).

**2. Synthetic methodology of Anisotropic Au/Si Janus Nanoparticles.** The suitability of the nanoparticles as precursors to other nanomaterials was assessed by using them for the synthesis of Janus nanoparticles. A batch in the conditions of sample S3 was prepared (reaction time, 24 h). To clean the crude reaction, three cycles of centrifugation were done in acetonitrile (8000 rpm x 30 min). To remove the shell, the pellet was then re-suspended in 3 mL of ethanol. 1 mL of these "naked" gold nanoparticles were then used for the synthesis of Janus nanoparticles as follows. In a reaction flask over magnetic stirring, 5 mL of 2-propanol were added. Then, (i) 40 μL of a poly(acrylic acid) sodium salt solution in water (4.7 mg/mL), (ii) 40 μL of a 4-mercaptophenyl acetic acid solution in ethanol (7.3 mM), (iii) 3 mL of a tetraethylorthosilicate solution in propanol (9.9 mM), and finally, (iv) 4 mL of milliQ water were sequentially added. At this stage, the reaction medium showed a red/purple color. The sample was then subjected to ultrasound (10 s ultrasonic bath), and 100 μL of 28% $NH_4OH$ aqueous solution were added immediately after. The color changed to ruby red, indicating the total removal of the organotellurium outer shell residue. Finally, the reaction medium was kept over magnetic stirring during 12 h. Several centrifugation cycles in ethanol and water were then performed (8000 rpm x 30 min) to obtain the pure nanomaterial.

**3. Electrophoresis and 1D-SDS-PAGE (sodium dodecyl sulfate polyacrylamide gel electrophoresis).** Protein electrophoresis was carried out using the PROTEAN Tetra Cell from Bio-Rad (USA). Gel image acquisition and spot picking were performed using a PROPIC II DigiLab Genomic Solutions (USA). Protein samples were mixed with 5 μL of sample buffer (SB, 65.8 mM Tris–HCl pH 6.8, 2.1% SDS (w/v), 26.3% (w/v) glycerol, 0.01% (w/v) of bromophenol blue and 10% (v/v) β-mercaptoethanol) and then heated in a dry bath at 100ºC for 5 minutes. The denatured proteins were loaded in 12.5% polyacrylamide gels with 1 mm thickness. Proteins were separated at 200 V (constant voltage) until the tracking dye front reaches the bottom of the gel. Finished the gel electrophoresis, the gel was fixed for 30 minutes with 40% (v/v) ethanol and 10% (v/v) acetic acid and then stained overnight with colloidal coomassie blue G-250. Gels were rinsed 4×20 min with 100 mL of distilled water and further washed twice with 100 mL of 0.5 M sodium chloride until a clear background was observed. Gel imaging was carried out with a ProPicII–robot using 16 ms of

exposure time and a resolution of 70 µm.

**4. Conversion efficiency of Au(III) into AuNPs**

To estimate the conversion efficiency of Au(III) into Au nanoparticles have been analyzed the solid residue of the supernatant reaction. To this end, a reaction batch under S3 conditions was prepared, proceeding to a quick centrifugation of the reaction medium after 30 minutes of reaction (14000 rpm×10 min). The solvent was evaporated, and the solid residue was dry under vacuum. The ICP analysis revealed a gold content of 0.018% (0.003 mg). The initial content of Au(III) in a typical reaction was equal to 3.93 mg ($2.10^{-5}$ Au(III), Mw=196.665gr/mol). Based on this result, and assuming that the total gold collected in the pellet is in the form of nanoparticles, and the gold present in the supernatant is in the form of Au(III) the conversion efficiency obtained was 99.92%.

**5. Additional characterization**

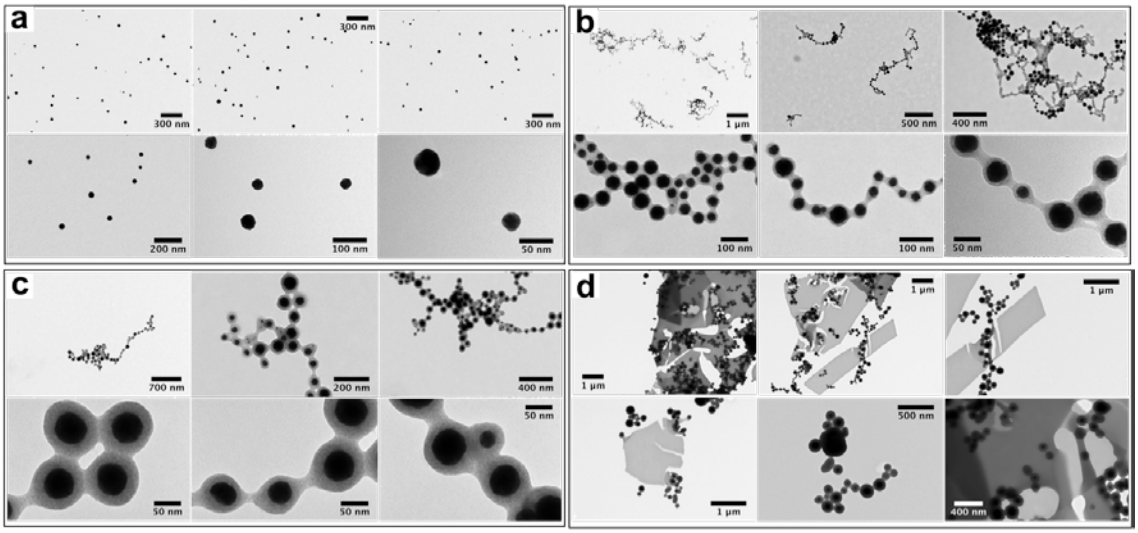


**Figure S1.** Effect of water in the formation of the Au-Te nanoparticles. TEM images of samples **(a)** S1 (0% v/v $H_2O$), **(b)** S2 (0.1% v/v $H_2O$), **(c)** S3 (0.2% v/v $H_2O$) and **(d)** S4 (0.4% v/v $H_2O$) after 24 h of reaction. The samples were isolated by centrifugation at 8000 rpm x 30 minutes, and then the pellet re-suspended in acetonitrile. A second cycle of centrifugation was done for each sample. For TEM analysis, the samples were re-suspended in acetonitrile.

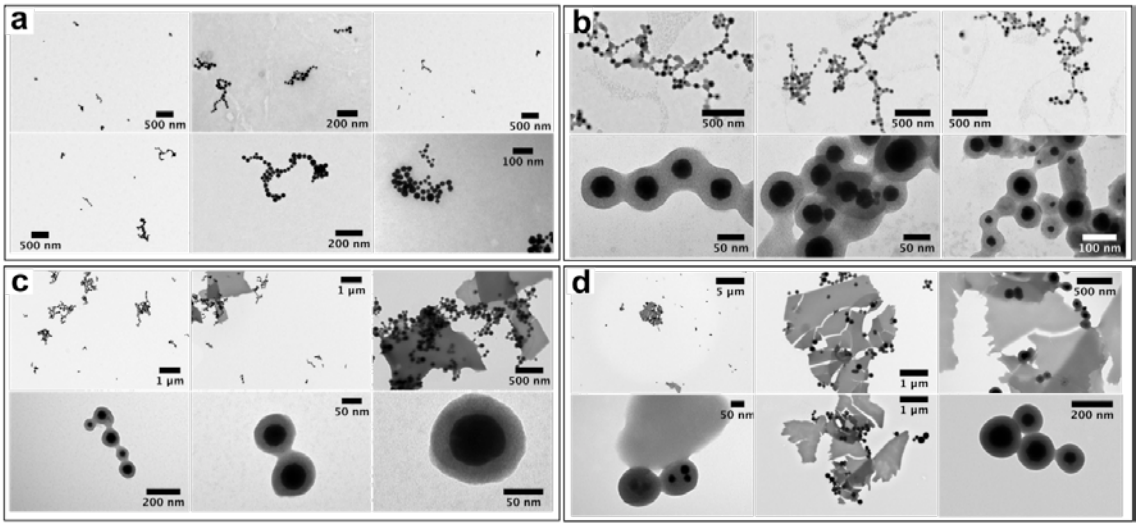


**Figure S2.** Effect of water in the formation of the Au-Te nanoparticles. TEM images of samples **(a)** S1 (0% v/v $H_2O$), **(b)** S2 (0.1% v/v $H_2O$), **(c)** S3 (0.2% v/v $H_2O$) and **(d)** S4 (0.4% v/v $H_2O$) after 48 h of reaction.

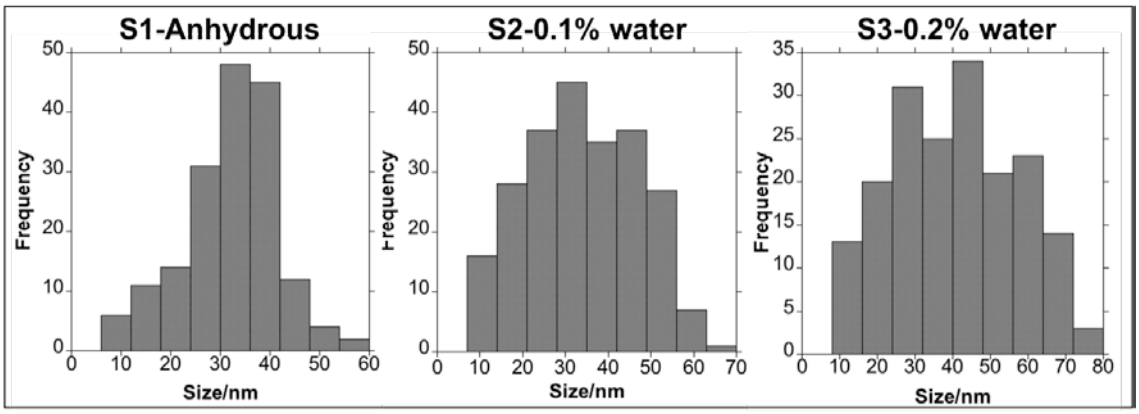


**Figure S3.** Effect of water in the formation of the Au-Te nanoparticles. Particle size histograms for sample S1 (0% v/v $H_2O$), S2 (0.1% v/v $H_2O$) and S3 (0.2% v/v $H_2O$) after 24 h reaction. The histograms show the effect of water content in core size growth. Monodispersity is higher in the anhydrous condition (S1).

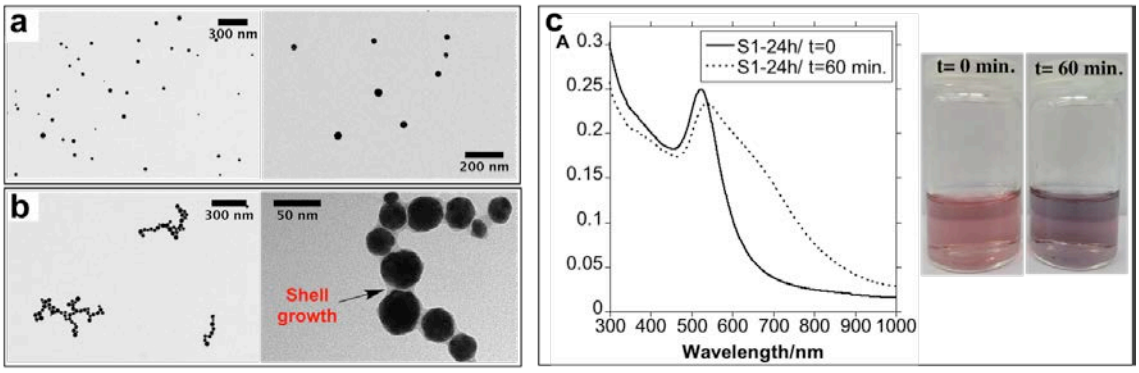


**Figure S4.** Effect of water in the formation of the Au-Te nanoparticles. TEM images for nanoparticles synthesised in condition S1 (0% v/v $H_2O$), re-suspended in acetonitrile at **(a)** t=0 min and **(b)** t=60 min, showing shell formation at 60 min, due to $Ph_2Te_2$ traces present. **(c)** Spectroscopic profile and color solution of isolated NPs S1-24h in acetonitrile from t=0 to t=60 min; both the red shift in the Surface Plasmon Resonance band (SPRB) at ca. 530 nm at t= 60 min, and the change in the color of the solution, indicate shell formation.

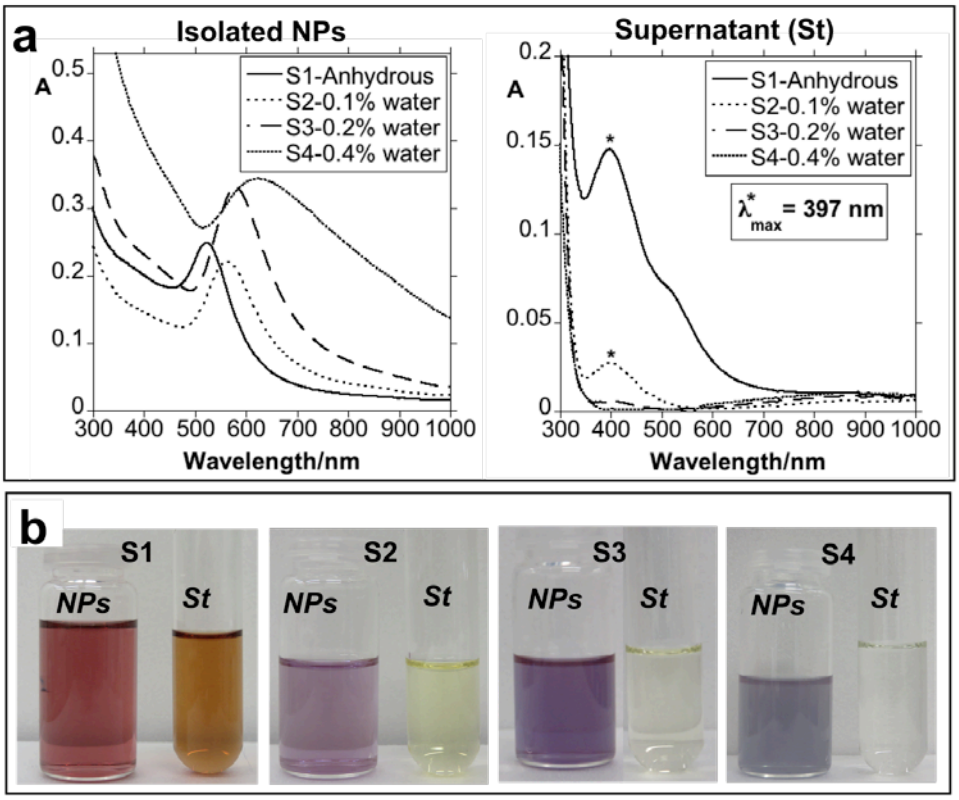


**Figure S5.** Effect of water in the formation of the Au-Te nanoparticles. **(a)** UV-vis spectroscopic profiles of isolated nanoparticles (NPs) in acetonitrile and supernatants (St) (dilution 1/3 in acetonitrile) for conditions S1 (0% v/v $H_2O$), S2 (0.1% v/v $H_2O$), S3 (0.2% v/v $H_2O$) and S4 (0.4% v/v $H_2O$) after 24h of reaction. The UV-vis profiles of the supernatant show a decrease of the band centered at c.a. 397 nm as a function of the amount of water present in the reaction media; this band is attributable to a charge transfer (CT) band between both Te-Te units in the precursor. Part **(b)** shows the color of the solutions for each condition.

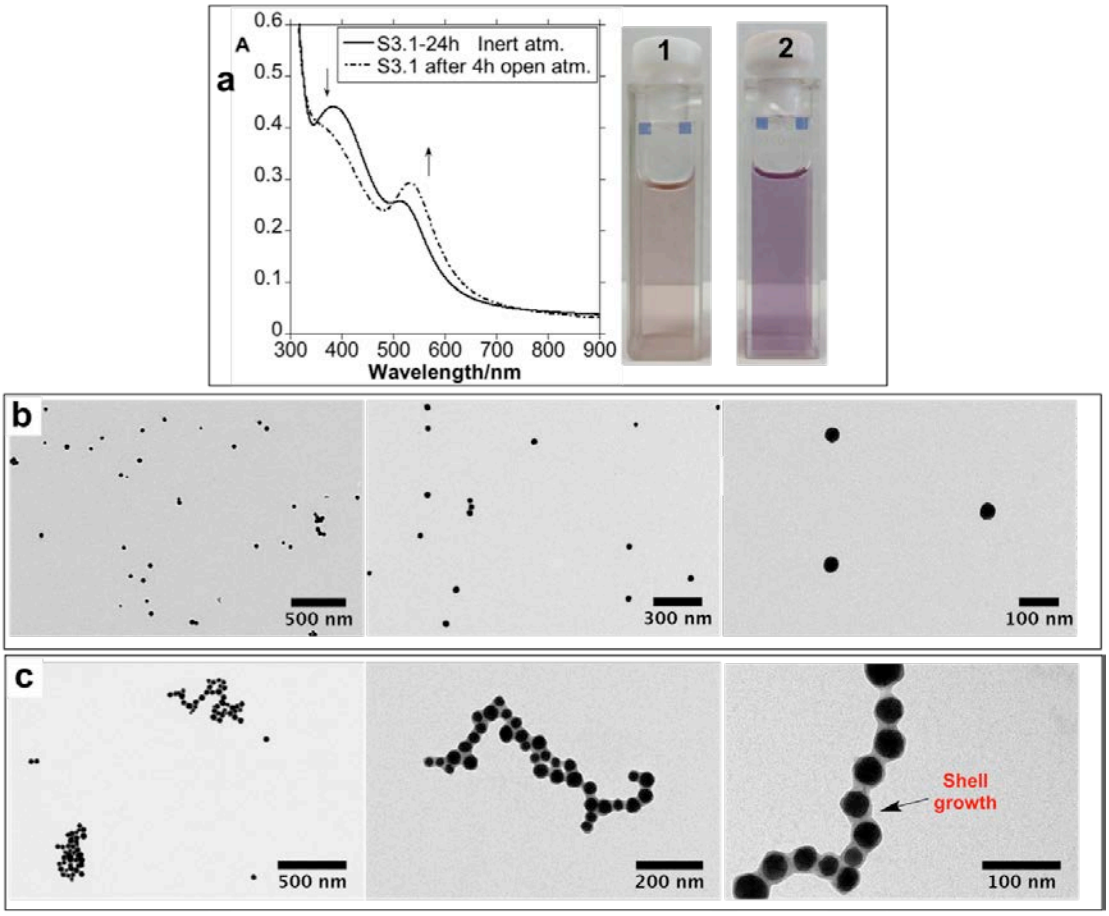


**Figure S6.** Effect of oxygen in the formation of the Au-Te nanoparticles: synthesis of S3.1 (0.2% v/v $H_2O$, synthesized in nitrogen atmosphere, 24 h). **(a)** UV-vis absorption spectrum (left) and color solution (right) for S3.1 (solid line), and then after 4 h exposed to open atmosphere with magnetic stirring (dashed line). A redshift in the SPRB at 533 nm is observed, indicating the growth of the shell when the solution is exposed to oxygen; moreover, the band at ca. 400 nm (attributable to the Te precursor) decreases, indicating shell formation. A change in the color of the solution can also be observed. **(b)** TEM images for sample S3.1, in which no shell formation is observed. **(c)** TEM images for sample S3.1 after 4 h in open atmosphere; shell growth can be observed.

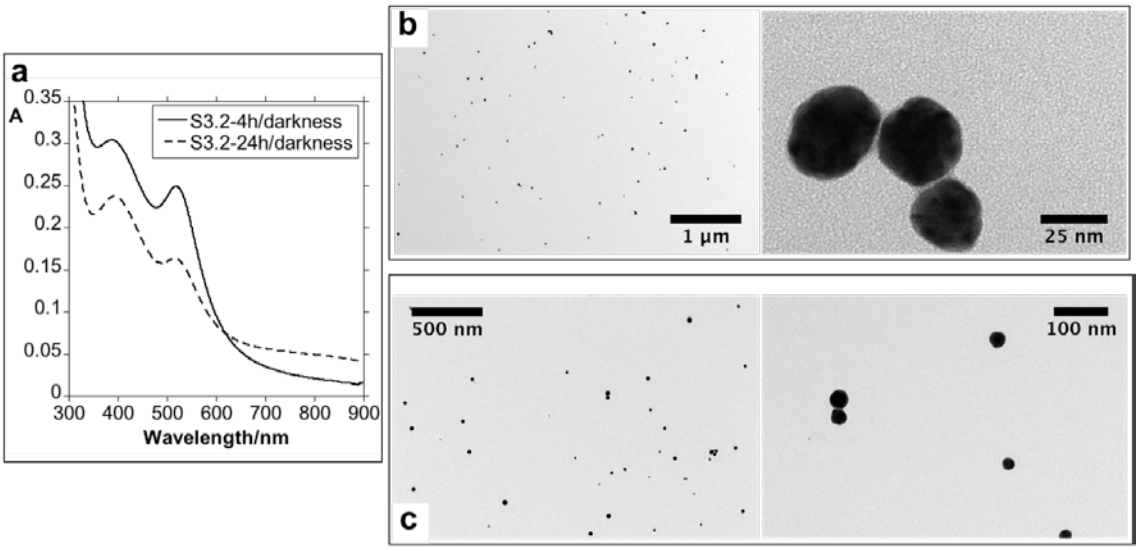


**Figure S7.** Effect of light in the formation of the Au-Te nanoparticles: synthesis of S3.2 (0.2% v/v $H_2O$, synthesized in the dark). **(a)** Absorption spectra of the reaction mixture after 4h (solid line) and 24h (dashed line) of synthesis in the dark. TEM images of sample S3.2 at 4h **(b)** and 24h **(c)** of reaction. Both UV-vis and TEM results show the lack of the shell formation.

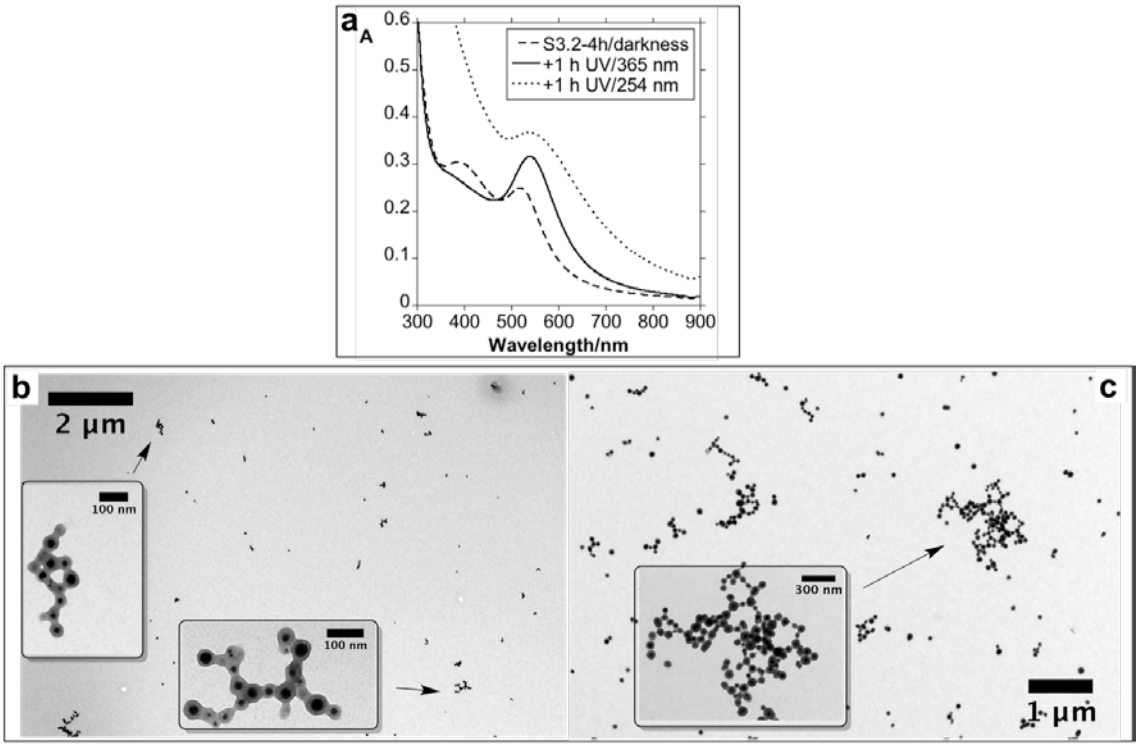


**Figure S8.** Effect of light in the formation of the Au-Te nanoparticles: synthesis of S3.2 (0.2% v/v $H_2O$, synthesized in the dark). Two aliquots from the sample synthesised in the dark were taken after 4 h of reaction, and irradiated for 1 h at 365 and 254 nm respectively. **(a)** Absorption spectra for S3.2 (dashed line), S3.2 irradiated at 365 nm (solid line) and S3.2 irradiated at 254 nm (dotted line). **(b)** TEM images of the sample irradiated at 365 nm. **(c)** TEM images of the sample irradiated at 254 nm. Shell formation can be seen for both wavelengths.

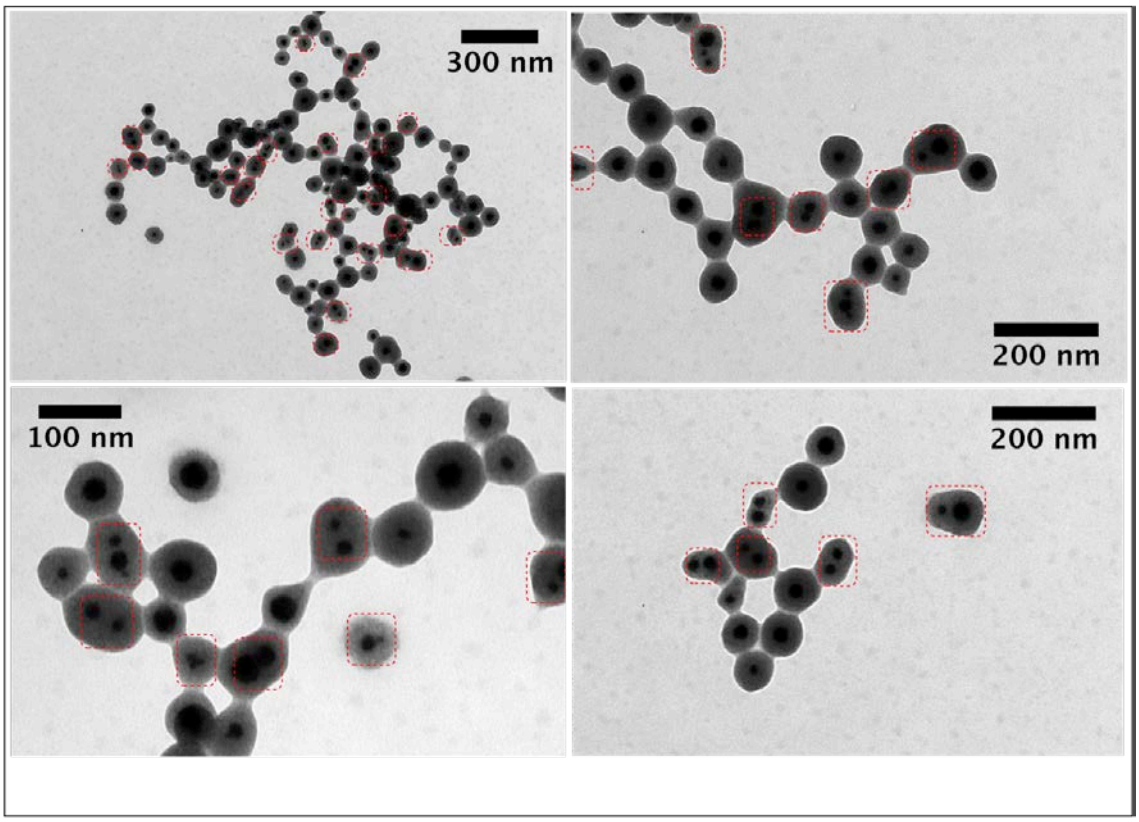


**Figure S9.** Effect of light in the formation of the Au-Te nanoparticles: synthesis of S3.2 (0.2% v/v $H_2O$, synthesised in the dark). TEM images of sample S3.2 (4 h synthesis) after being at 254 nm for an hour. Red boxes indicate dimeric and trimeric Au cores.

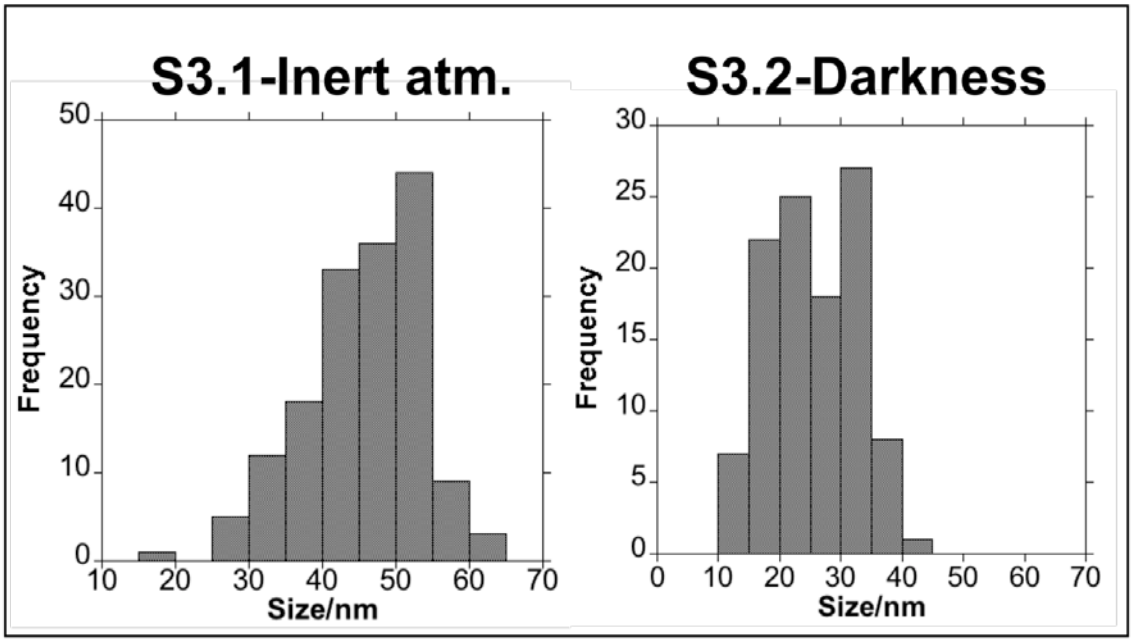


**Figure S10:** Effect of light and oxygen in the formation of the Au-Te nanoparticles. Particle size histograms for S3.1 (0.2% v/v $H_2O$, synthesized in nitrogen atmosphere) and S3.2 (0.2% v/v $H_2O$, synthesised in the dark), both after 24 h of reaction.

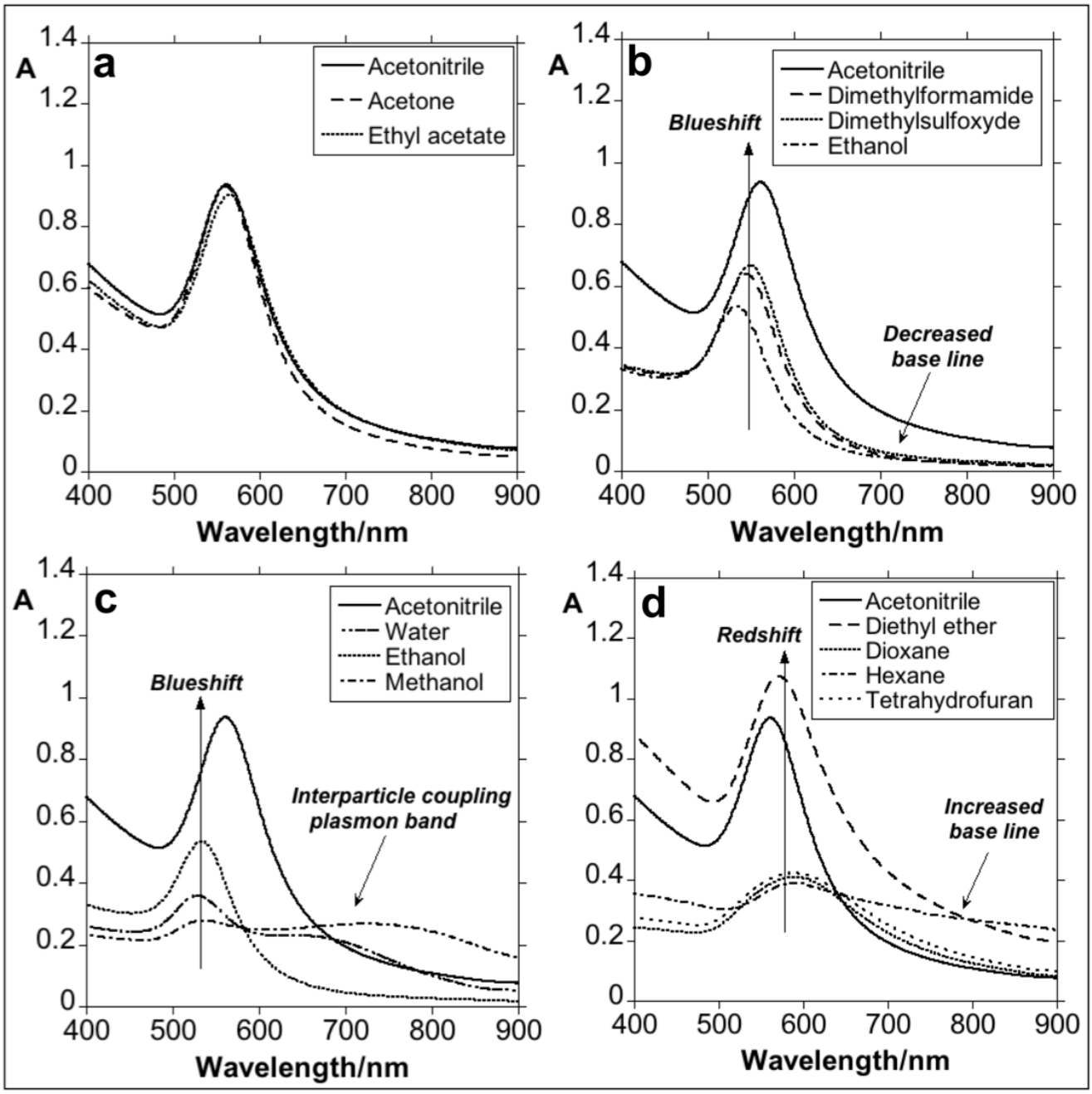


**Figure S11.** Spectroscopic study of sample S3 (0.2% $H_2O$) in different solvents. **(a)** The spectroscopic profiles in acetone and ethyl acetate are similar to that of acetonitrile, with a similar polymeric coating and shell stability. **(b)** The profiles in dimethylsulfoxide and dimethylformamide show a blue shift with a decreasing baseline, a similar behaviour to that of absolute ethanol; this suggests the presence of more polymeric coating shell over the surface of the nanoparticles, perhaps due to the largely high hygroscopic

nature of these both solvents in regular conditions. **(c)** The UV-vis blue shift observed in methanol and water is comparable with that of absolute ethanol, indicating the solubilisation of the shell. Both solvents show a noticeable decrease in the SPRB (*ca.* 525 nm), and the appearance of a coupling plasmon band; we hypothesise that the monolayer formed in these solvents does not stabilize the nanoparticle. **(d)** Diethyl ether, tetrahydrofuran, hexane and dioxane produce a red shift and a baseline increase; this behaviour may be due to the low solubility of the polymeric outer shell in such solvents. A solid deposition appeared on the walls of the flask during the re-suspension of the nanoparticles in hexane, dioxane and tetrahydrofuran, indicating of lower stability in those solvents.

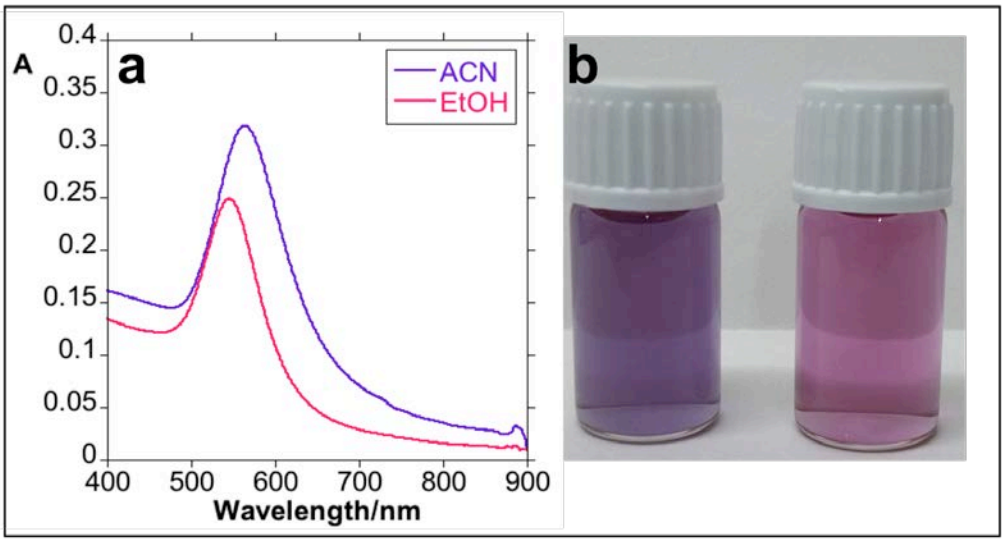


**Figure S12. (a)** Absorption spectra and **(b)** color of the solutions of isolated Au-Te nanoparticles with more than seven months after be synthesized (condition S3, storage in acetonitrile solution), dissolved in acetonitrile (ACN) and ethanol (EtOH).

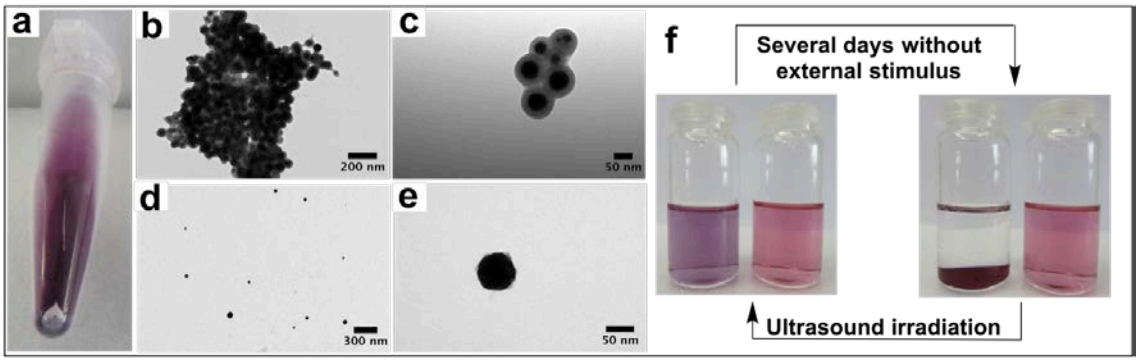


**Figure S13.** Dry sample and colloid coalescence. **(a)** S3 sample (0.2% $H_2O$) dried for long-term storage; **(b, c)** TEM image of the dry sample re-suspended in acetonitrile; **(d, e)** TEM image of the dry sample re-suspended in absolute ethanol; **(f)** colloidal system dissolved in acetonitrile (left side of both images) or absolute ethanol (right side of both images). In acetonitrile, the Au-Te nanoparticles coalesce after few days, and can be re-suspended using ultrasound; coalescence is not observed in ethanol, with the solution being stable for months.

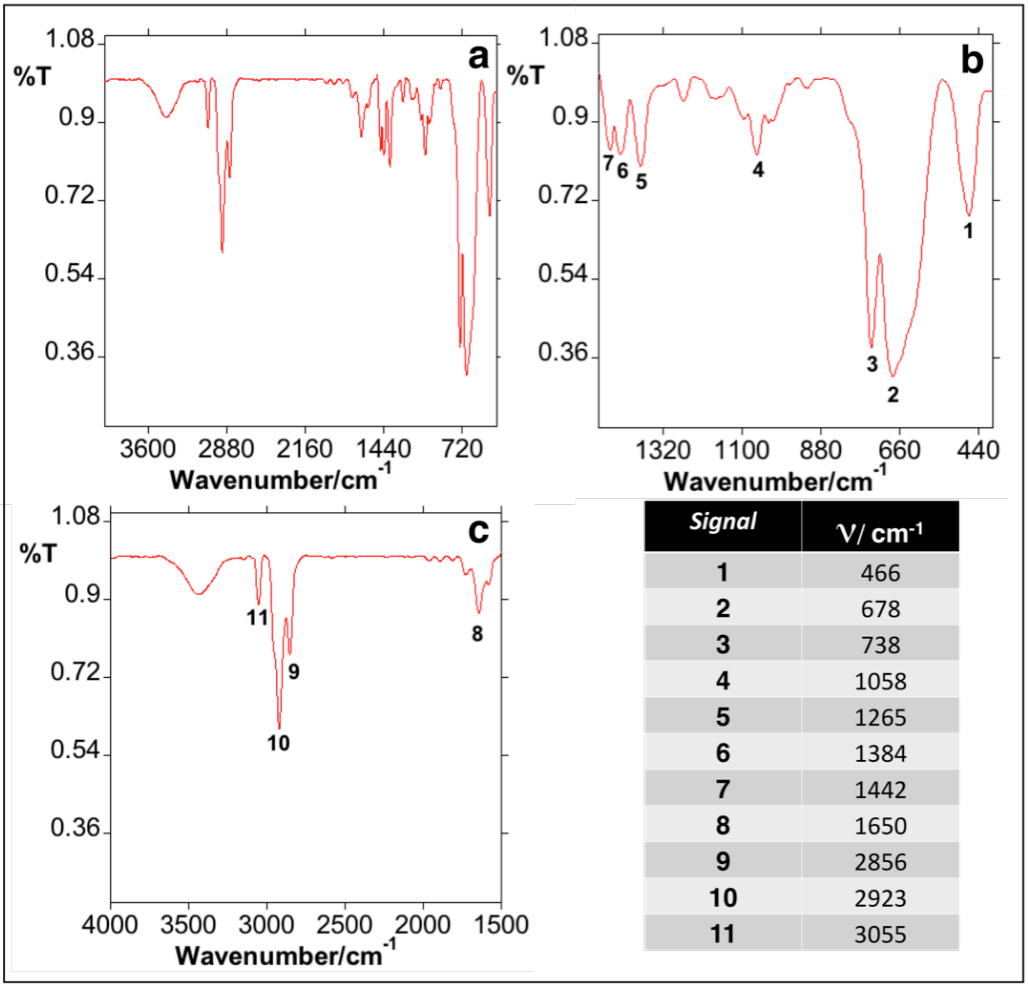


| Signal | ν/ cm-1 |
|---|---|
| 1 | 466 |
| 2 | 678 |
| 3 | 738 |
| 4 | 1058 |
| 5 | 1265 |
| 6 | 1384 |
| 7 | 1442 |
| 8 | 1650 |
| 9 | 2856 |
| 10 | 2923 |
| 11 | 3055 |

**Figure S14.** Fourier transform infrared (FT-IR) spectroscopy analysis of the Te shell **(a)** full spectrum and **(b, c)** sections showing typical signals for tellurinic anhydride derivatives, as reported in the literature.[1]

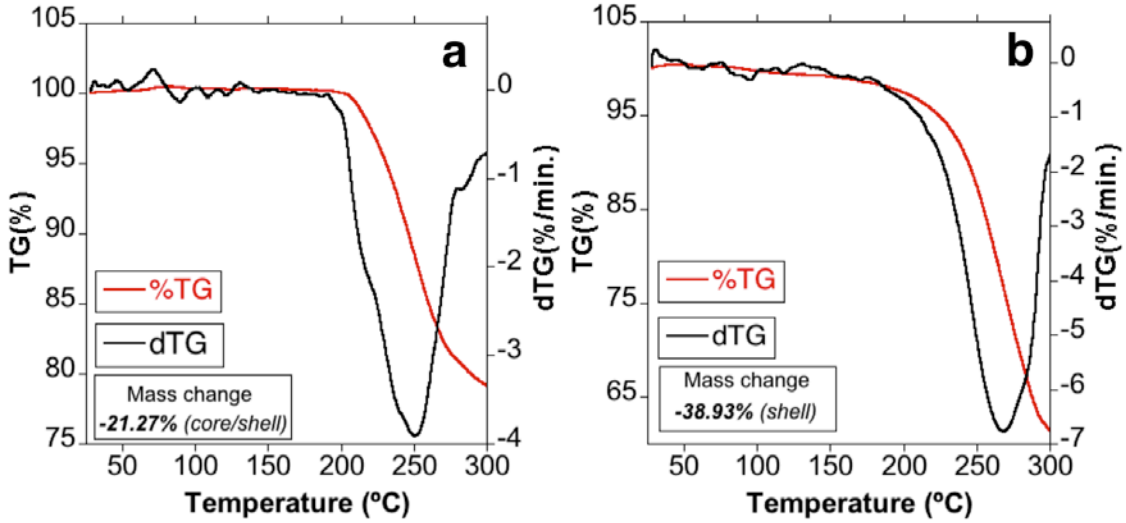


**Figure S15.** TGA and dTG spectra of **(a)** core/shell and **(b)** isolated shell

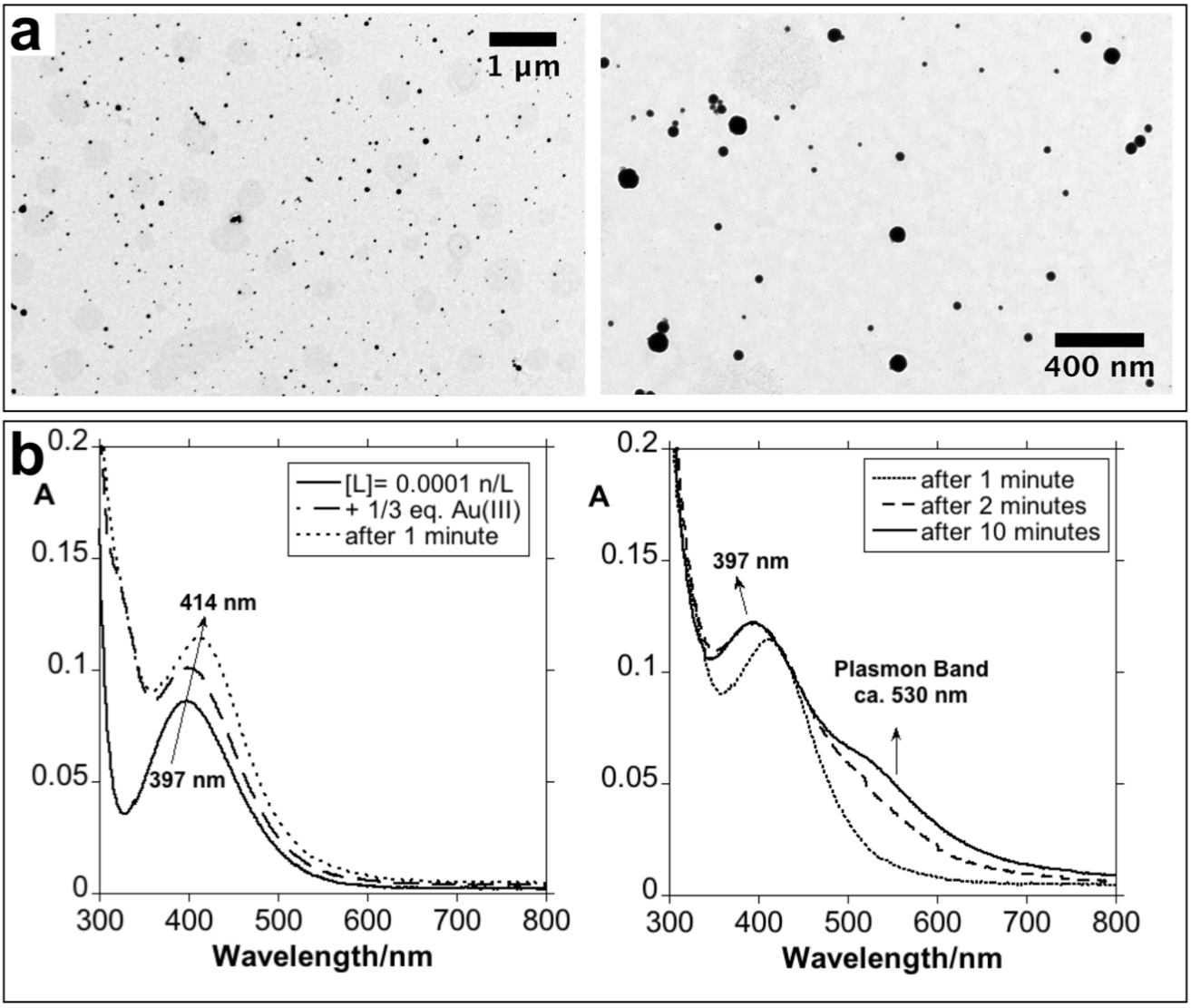


**Figure S16. (a)** TEM images of the nanoparticles obtained in the 1:1 (L:Au) kinetic study. **(b)** Kinetic study of the interaction 3:1 (L: Au). UV/Vis study of the interaction of $Ph_2Te_2$ ([L]=$1.10^{-4}$M) with addition of 1/3 equivalent of $HAuCl_4$ in acetonitrile solution; stabilization occurs after the first 10 minutes of reaction.

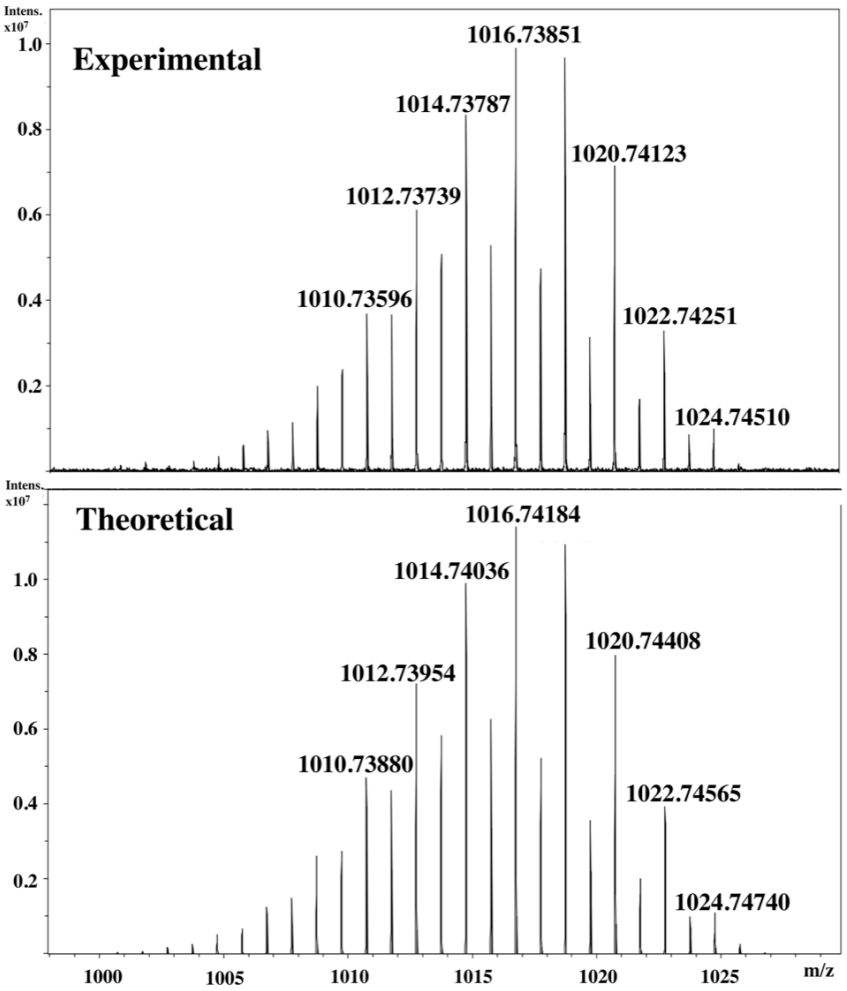


**Figure S17.** FT-ICR mass spectrometry studies. Experimental and theoretical isotopic pattern for the 1016.738 m/z signal, attributable to a molecular complex with empirical formula of $[C_{24}H_{20}Te_4Au]^+$.

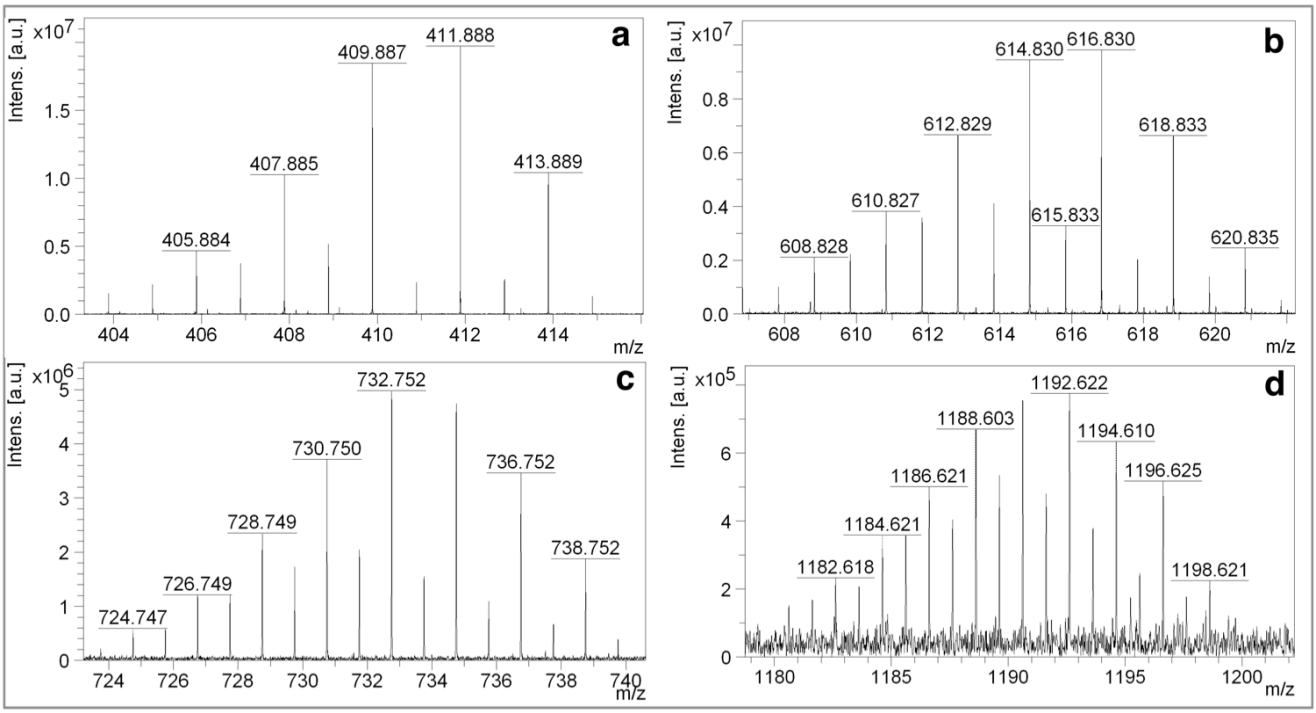


**Figure S18.** FT-ICR mass analysis. Experimental isotopic mass spectra for the peaks at m/z 411.888 **(a)**, 616.830 **(b),** 732.752 **(c)** 1192.622 **(d)**.

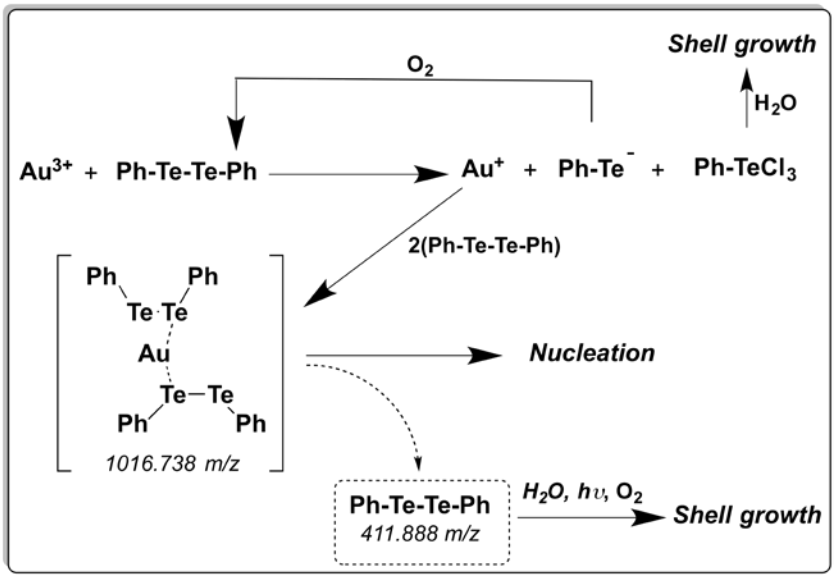


**Figure S19**. Proposed mechanism for the formation of the Au-Te complex and shell growth.

## 5. References

[1] Oba, M.; Nishiyama, K.; Koguchi, S.; Shimada, S.; Ando, W. *Synthesis and Properties of Tellurinic Anhydride–Tellurone Adducts.* Organometallics **2013**, 32, 6620–6623.